




Calculated magnetic exchange interactions in the quantum spin chain materials $\text{K}_2\text{CuSO}_4\text{Cl}_2$ and $\text{K}_2\text{CuSO}_4\text{Br}_2$

Xiangyan Bo , Di Wang,^{*} Bo Wan , and X. G. Wan

National Laboratory of Solid State Microstructures and School of Physics, Nanjing University, Nanjing 210093, China and Collaborative Innovation Center of Advanced Microstructures, Nanjing University, Nanjing 210093, China

 (Received 12 October 2019; revised manuscript received 22 December 2019; published 21 January 2020)

Using density functional calculations, we present a comprehensive study of the electronic and magnetic properties of the quantum spin chain materials $\text{K}_2\text{CuSO}_4\text{Cl}_2$ and $\text{K}_2\text{CuSO}_4\text{Br}_2$. With the first-principles linear response method, we calculate the magnetic exchange parameters, and the theoretical values are in a quantitatively good agreement with experiments. Depending on the signs and magnitudes of the interchain magnetic exchange interactions, we find that the magnetic order of $\text{K}_2\text{CuSO}_4\text{Br}_2$ along the b axis is antiferromagnetic, while $\text{K}_2\text{CuSO}_4\text{Cl}_2$ has strong frustration along the b axis. Based on the obtained magnetic exchange parameters, we successfully reproduce the experimental spin-wave dispersion. We also calculate Dzyaloshinskii-Moriya interactions, which are found to dominate in these compounds compared to the interchain magnetic exchange interactions. Finally, we obtain the phase diagram for these two materials using Monte Carlo simulations. Our results are consistent with previous experiments, giving a complete explanation of the magnetic structure.

DOI: [10.1103/PhysRevB.101.024416](https://doi.org/10.1103/PhysRevB.101.024416)

I. INTRODUCTION

For a long time, low-dimensional quantum antiferromagnetics have gained great interest because some novel and peculiar quantum phases can be observed, such as spin liquids [1,2]. In recent years, an increasing number of spin- $\frac{1}{2}$ quasi-one-dimensional materials, mainly Cu^{2+} compounds, have been discovered, such as Cs_2CuCl_4 [3–8], Cs_2CuBr_4 [9–12], and LiCuVO_4 [13–21]. Besides the significant intrachain interactions, the interchain interactions are also important and can lead to magnetic long-range order, when the temperature drops below the Néel temperature T_N [22]. By constructing a model with one-dimensional spin chains, we can understand many interesting quantum magnets. Many of these quantum magnets are characterized by significant anisotropy of exchange interactions, such as uniform Dzyaloshinskii-Moriya (DM) interactions [23,24], staggered DM interactions [25], or disorders [26,27].

Recently, Hälg *et al.* [28] investigated a family of spin chain materials, $\text{K}_2\text{CuSO}_4\text{Cl}_2$ and $\text{K}_2\text{CuSO}_4\text{Br}_2$. The specific heat measurements reveal that the Néel temperature is about 77 mK for $\text{K}_2\text{CuSO}_4\text{Cl}_2$ and 100 mK for $\text{K}_2\text{CuSO}_4\text{Br}_2$ [28]. In addition, the most interesting feature is the presence of a uniform DM interaction in the intrachain exchange, and DM vectors are arranged antiparallel to each other in adjacent chains [28]. In general, DM interactions are caused by spin-orbit coupling (SOC) and could lead to noncollinearity of the magnetic ground state [29,30]. Although DM interactions have been shown to be weaker than intrachain exchange interactions, they are quite large compared to the interchain exchange interactions in these materials [28]. For example, for $\text{K}_2\text{CuSO}_4\text{Br}_2$, the electron spin resonance experiment

yields a value of $D = 0.28$ K, which is smaller than the intrachain exchange interaction ($J = 20.7$ K) measured by neutron scattering, and is larger than the interchain exchange interaction ($J' = 0.034$ K) calculated from the value of T_N [28]. On the other hand, Jin and Starykh [31] investigated this structure using the Heisenberg spin chain model and found that different D/J' ratios would result in completely different phase diagrams at low-temperature limits. Motivated by the theoretical prediction [31], Soldatov *et al.* [32] measured the spin gap of $\text{K}_2\text{CuSO}_4\text{Cl}_2$ with electron spin resonance experiments and estimated the value of DM interaction within the interval $0.06 < D < 0.16$ K. Compared to the strength of the DM interaction, the value of the interchain exchange interaction of $\text{K}_2\text{CuSO}_4\text{Cl}_2$ is more debatable. The direct measurement of inelastic neutron scattering in the saturated phase finds the interchain exchange value of 0.45 K for $\text{K}_2\text{CuSO}_4\text{Cl}_2$ [33], which is 15 times larger than the value (0.031 K) estimated from the value of T_N [28]. Moreover, Jin and Starykh [31] also calculated the interchain exchange interaction using the same data, but the value is different from that obtained by Hälg *et al.* [28]. Therefore, calculating accurate spin exchange parameters and DM interactions is an interesting issue, which we focus on in our current work.

In this work, based on first-principles calculations, we systematically study the electronic and magnetic properties of $\text{K}_2\text{CuSO}_4\text{Cl}_2$ and $\text{K}_2\text{CuSO}_4\text{Br}_2$. The calculations reveal that $\text{K}_2\text{CuSO}_4\text{Cl}_2$ and $\text{K}_2\text{CuSO}_4\text{Br}_2$ are both insulators, with band gaps of 2.56 and 2.10 eV, respectively. The calculated magnetic moments are $0.70\mu_B$ for $\text{K}_2\text{CuSO}_4\text{Cl}_2$ and $0.65\mu_B$ for $\text{K}_2\text{CuSO}_4\text{Br}_2$. Using the first-principles linear response (FPLR) method [34,35], we calculate the magnetic exchange parameters. There are four considerable magnetic exchange interactions, which are all antiferromagnetic. Based on the obtained magnetic exchange parameters, we calculate the spin-wave dispersion with the linear spin-wave theory, and

^{*}Corresponding author: diwang910214@gmail.com

the calculated results agree well with the experiment [28]. We also calculate the DM interactions, and the results indicate that the DM interactions are quite large compared to the interchain interactions in these materials, consistent with the previous experimental works [28,32]. Moreover, using Monte Carlo (MC) simulations, we study the phase diagrams of these two materials.

II. METHOD

The electronic band structure calculations have been carried out by using the full potential linearized augmented plane-wave method as implemented in the WIEN2K package [36]. The local spin-density approximation (LSDA) for the exchange-correlation potential has been used here. We utilize the LSDA+ U scheme [37] to take into account the effect of Coulomb repulsion in the Cu 3d orbital. For Cu oxides, the values are chosen as $U = 9 \pm 1$ eV and $J = 1$ eV from previous theoretical works [38–41]. Thus, we use an additional effective Hubbard $U_{\text{eff}} = U - J = 8$ eV in this work. Using the second-order variational procedure, we include the SOC interaction [42]. Here, we use the experimental lattice constants from Ref. [28] and optimize the internal atomic coordinate. The basic functions were expanded to $R_{mt} K_{\text{max}} = 7$, where R_{mt} is the smallest of the muffin-tin sphere radii and K_{max} is the largest reciprocal lattice vector used in the plane-wave expansion. A $5 \times 2 \times 2$ k -point mesh is used for the Brillouin zone integral. The self-consistent calculations are considered to be converged when the difference in the total energy of the crystal does not exceed 0.01 mRy at consecutive steps.

The exchange constants J are the basis to understand the magnetic properties. In order to obtain the exchange constants, the experimental results (for example, magnetization curves and magnon dispersion) are usually reproduced by fitting J . However, an unambiguous fitting is basically impossible. For example, as mentioned above, the interchain exchange constant J' obtained by Halg *et al.* is 0.031 K [28] while the value obtained by Jin and Starykh is about three times larger (0.083 K) [31], though their results are obtained from the same experimental data [28]. In addition, theoretical calculations can also be used to estimate exchange interactions. Here, we use an efficient first-principles method to calculate the magnetic exchange interactions, which is based on a combination of the magnetic force theorem and the linear response method [34]. We assumed a rigid rotation of atomic spin at sites $R + \tau$ and $R' + \tau'$ of the lattice (here R are the lattice translations and τ are the atoms in the basis). Then, the exchange interaction constant J can be given as a second variation of the total energy induced by the rotation of atomic spin at sites $R + \tau$ and $R' + \tau'$ [35],

$$J_{\tau R \tau' R'}^{\alpha\beta} = \sum_q \sum_{k j j'} \frac{f_{kj} - f_{k+qj'}}{\epsilon_{kj} - \epsilon_{k+qj'}} \langle \psi_{kj} | [\sigma \times B_{\tau}]_{\alpha} | \psi_{k+qj'} \rangle \times \langle \psi_{k+qj'} | [\sigma \times B_{\tau'}]_{\beta} | \psi_{kj} \rangle e^{iq(R-R')}, \quad (1)$$

where σ and B are the Pauli matrix and the effective local magnetic field, respectively. ϵ is the one-electron energy while ψ is the corresponding wave function. With the electronic structure information from the LSDA+ U calculation, one can evaluate the magnetic exchange interactions by using Eq. (1).

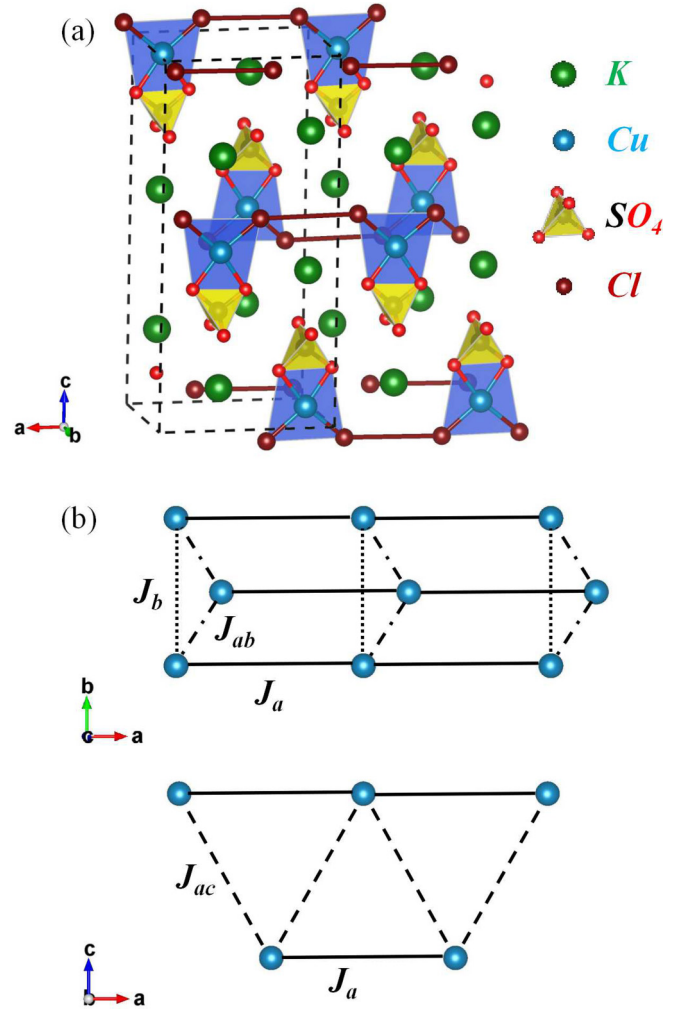


FIG. 1. (a) Crystal structure of $\text{K}_2\text{CuSO}_4\text{Cl}_2$. (b) The nearest-neighbor, next-nearest-neighbor, and fourth-nearest-neighbor interchain exchange interactions and intrachain exchange interaction for Cu magnetic moments shown by J_{ab} , J_b , J_{ac} , and J_a , respectively.

This method has been successfully used to evaluate magnetic interactions, including DM interactions in a range of materials [34,35,38,43–47]; therefore, we apply this method to calculate the magnetic exchange interactions of $\text{K}_2\text{CuSO}_4\text{Cl}_2$ and $\text{K}_2\text{CuSO}_4\text{Br}_2$ in this paper.

III. RESULTS AND DISCUSSION

As shown in Fig. 1(a), $\text{K}_2\text{CuSO}_4\text{Cl}_2$ crystallizes in an orthorhombic $Pnma$ structure [48]. The lattice constants of $\text{K}_2\text{CuSO}_4\text{Cl}_2$ are $a = 7.73$ Å, $b = 6.08$ Å, and $c = 16.29$ Å [28]. $\text{K}_2\text{CuSO}_4\text{Br}_2$ was grown in the same structure. The lattice constants of $\text{K}_2\text{CuSO}_4\text{Br}_2$ are $a = 7.73$ Å, $b = 6.30$ Å, and $c = 16.43$ Å [28]. The details of the crystal structure are described in Fig. 1. The crystal structure of chlorosulfate consists of a CuO_2Cl_2 quadrilateral and a SO_4 tetrahedron [48]. The CuO_2Cl_2 quadrilateral is located in a plane perpendicular to the b axis, and the bond angle around the copper atom is strongly distorted. Sulfate SO_4 is approximately a regular tetrahedron. The SO_4 tetrahedron is connected to the Cu quadrilateral by two oxygen atoms. Because of their

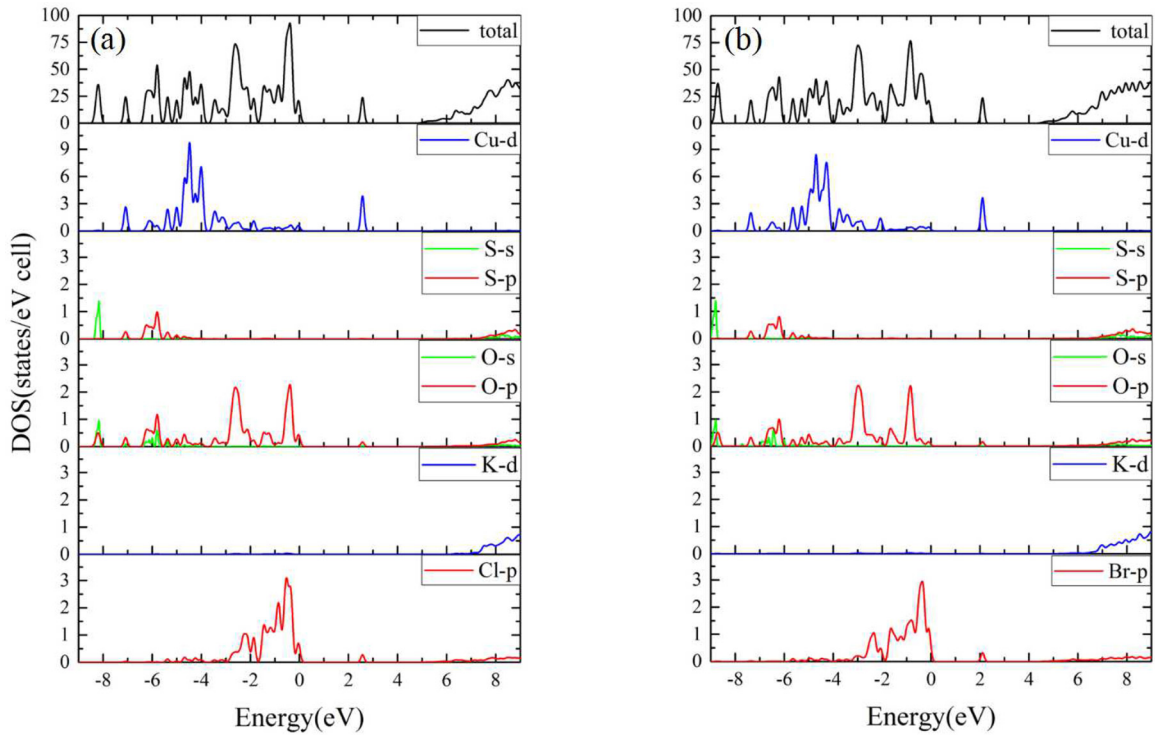


FIG. 2. Partial density of states of (a) $\text{K}_2\text{CuSO}_4\text{Cl}_2$ and (b) $\text{K}_2\text{CuSO}_4\text{Br}_2$ from the LSDA+ U ($= 8$ eV) calculation. The Fermi energy is set to zero.

electrostatic repulsion, S and Cu are pushed in opposite directions, respectively. In addition, there are two symmetrical independent K atoms located on the plane of the CuO_2Cl_2 quadrilateral. Each cell contains four Cu ions, each of which extends along the a axis as an antiferromagnetic spin chain [48]. The neutron powder diffraction experiments show that the intrachain exchange interaction is antiferromagnetic, and the nearest-neighbor interchain exchange interaction along the b axis is also antiferromagnetic [28]. Based on the structure and magnetic configuration suggested by the experiment [28,48], we perform the first-principles calculations.

With the LSDA+ U ($= 8$ eV) calculations, we show the density of states (DOS) of $\text{K}_2\text{CuSO}_4\text{Cl}_2$ and $\text{K}_2\text{CuSO}_4\text{Br}_2$ in Fig. 2. Our calculations show that $\text{K}_2\text{CuSO}_4\text{Cl}_2$ and $\text{K}_2\text{CuSO}_4\text{Br}_2$ are both insulators with band gaps of 2.56 and 2.10 eV, respectively. For chloride, the Cl $3p$ states are mainly located between -3.0 and 0.0 eV, while the O $2p$ states are distributed between -9.0 and 0.0 eV. Thus, the bands near the Fermi level are mainly contributed by chlorine and oxygen atoms. The S $3s$ and $3p$ electrons have a significant covalency with the ligand oxygens, which bring the bonding state in between -9.0 and -5.5 eV. The nominal valence for K is $+1$ and that for Cl is -1 , while the nominal valence of SO_4 is -2 . Hence, the nominal valence of Cu is $+2$, which means there are nine occupied states and one unoccupied state for the $3d$ orbit. The occupied states of Cu ions are mainly located between -5.5 and -4.0 eV and the unoccupied state appears around 2.5 eV, indicating that there is a non-negligible hybrid between Cu and O. On the contrary, the K states are far away from the Fermi level, mainly above 6.0 eV. As shown in Fig. 2, the DOS of $\text{K}_2\text{CuSO}_4\text{Br}_2$ shows similar behavior

as that of $\text{K}_2\text{CuSO}_4\text{Cl}_2$. Since the electronegativity of the Br atom is smaller than that of the Cl atom, the degree of hybridization of Cu-Br is higher than that of Cu-Cl. As a result, the band gap of $\text{K}_2\text{CuSO}_4\text{Br}_2$ is smaller than the band gap of $\text{K}_2\text{CuSO}_4\text{Cl}_2$. The calculated magnetic moment on the Br atom ($0.06\mu_B$) is larger than that on the Cl atom ($0.05\mu_B$), while the calculated magnetic moment on the Cu atom of $\text{K}_2\text{CuSO}_4\text{Br}_2$ ($0.65\mu_B$) is smaller than that of $\text{K}_2\text{CuSO}_4\text{Cl}_2$ ($0.70\mu_B$). Both the calculated magnetic moments of the Cu ions for $\text{K}_2\text{CuSO}_4\text{Cl}_2$ and $\text{K}_2\text{CuSO}_4\text{Br}_2$ are smaller than the experimental value of $1.1\mu_B$ [28].

As shown in Fig. 1(b), we depict the main magnetic interactions. The fourth-nearest-neighbor exchange path (J_d) is mediated by the Cu-X-X-Cu ($X = \text{Cl}, \text{Br}$) bond and produces a spin chain along the a axis. The interchain exchange interaction J_{ac} along the $[101]$ direction is the fifth-nearest-neighbor and can be expected to be weak due to the long distance. In addition, the nearest-neighbor J_{ab} and next-nearest-neighbor J_b exchange interactions are along the b axis and maybe lead to a frustrated spin chain along b . By neutron-scattering measurements, the experiments give the value of the interchain exchange constants J_{ab} , and the order of magnitude is about 0.1 K [28,33]. Based on the calculated electronic structures, we estimate the magnetic exchange interactions using the FPLR approach [35]. Considering that the magnetic exchange parameters are so small, we have taken different k -point meshes and the calculated values are almost the same. We list all the considerable exchange interactions in Tables I and II. The fitting magnetic exchange parameters from previous experimental works are also shown for comparison [28,31–33,49].

TABLE I. Calculated magnetic exchange parameters (in K) of $\text{K}_2\text{CuSO}_4\text{Cl}_2$ evaluated from the LSDA+ U ($= 8$ eV) scheme. The fitting magnetic exchange parameters in the experimental works are also presented for comparison.

	Expt.	This work
J_a	3.2, ^a 2.9, ^a 3.1, ^a 2.94 ^b	3.14
J_{ab}	0.2, ^a 0.031, ^a 0.073, ^c 0.083, ^d 0.45 ^b	0.03
J_b		0.03
J_{ac}		0.37
D_a^y	0.04, ^a 0.06, ^c 0.16 ^e	0.11

^aReference [28].

^bReference [33].

^cReference [49].

^dReference [31].

^eReference [32].

For $\text{K}_2\text{CuSO}_4\text{Cl}_2$, it can be seen from Table I that the intrachain exchange interaction J_a dominates over the others in strength, which determines the magnetic ground state. Our J_a (3.14 K) is consistent with the average of the values (3.1 K) obtained by thermodynamic and neutron measurements [28] and is slightly smaller than the fitting results (3.2 K) of the magnetic susceptibility curve [28]. The measurement of neutron scattering gives the value of 2.94 K [28,33], which is smaller than our J_a . In addition, our interchain exchange interaction J_{ab} (0.03 K) agrees well with the result from ordering temperature estimates (0.031 K) [28], but is smaller than the fitting results of the neutron-scattering measurements (0.45 K) [33]. Note that both the exchange constants J_{ab} and J_b are antiferromagnetic and there is competition between these two exchange interactions along the b axis, which results in frustration. Using the FPLR approach, we also calculate the DM interactions. The intrachain DM interaction D_a is estimated to be (0, 0.11, 0) K. The direction of D_a is parallel to the b axis direction, which is consistent with the requirements of symmetry analysis. Our calculated D_a^y is consistent with the results of the electron spin resonance experiment, and the value is in the range $0.06 < D_a^y < 0.16$ K [32].

Turning to the discussion of $\text{K}_2\text{CuSO}_4\text{Br}_2$, both our calculated J_a and D_y are much larger than that of $\text{K}_2\text{CuSO}_4\text{Cl}_2$, which is consistent with the experimental results [28]. Our J_a (16.17 K) is smaller than the average of the values (20.5 K)

TABLE II. Calculated magnetic exchange parameters (in K) of $\text{K}_2\text{CuSO}_4\text{Br}_2$ evaluated from the LSDA+ U ($= 8$ eV) scheme. The fitting magnetic exchange parameters in the experimental works are also presented for comparison.

	Expt.	This work
J_a	20.4, ^a 20.7, ^a 20.5 ^a	16.17
J_{ab}	0.034, ^a 0.20, ^b 0.091 ^c	1.06
J_b		0.03
J_{ac}		0.20
D_a^y	0.28 ^a	0.49

^aReference [28].

^bReference [49].

^cReference [31].

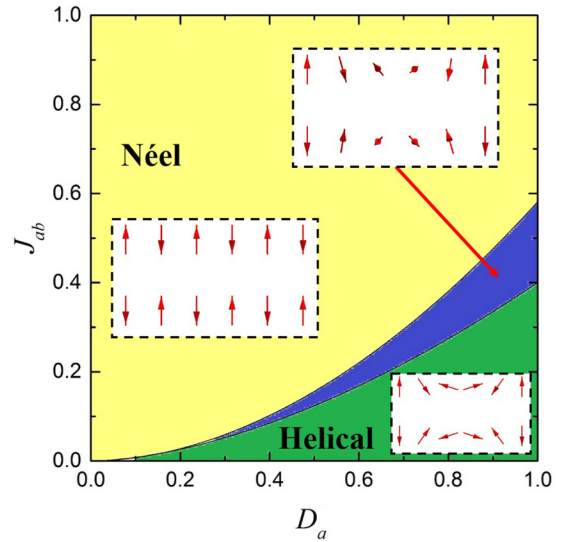


FIG. 3. The phase diagram obtained by the MC calculation. Here all the exchange interactions are in units of J_a . The insets show the schematic diagram of the spin configuration.

obtained by thermodynamic and neutron measurements [28]. On the contrary, our D_y (0.49 K) is larger than the results (0.28 K) of the electron spin resonance experiment [28]. Unlike $\text{K}_2\text{CuSO}_4\text{Cl}_2$, the J_{ab} of $\text{K}_2\text{CuSO}_4\text{Br}_2$ is much larger than J_b ($J_{ab}/J_b \approx 30$), resulting in an antiferromagnetic sequence along the b axis. One may naively expect that lower interchain exchange constants will lead to lower Néel temperature, but because the interactions between the various chains are all antiferromagnetic, the situation is more complicated.

For these two materials, the obtained intrachain and interchain interactions are all antiferromagnetic. When DM interaction is negligible, the magnetic ground state should be Néel order. On the contrary, for a single chain, the DM interaction would make the spins to favor a helical order, and the helical period depends on the value of D/J . However, the DM interactions of adjacent chains are antiparallel to each other, and the corresponding helical chains propagate in opposite directions. The competition between the interchain and DM interactions leads to a special kind of geometric frustration [28].

Unfortunately, to our best knowledge, the magnetic ground states of these two materials are not available currently and are waiting for future neutron diffraction or local probe experiments [28]. In order to better understand the competition between interchain and DM interactions, we employ an effective spin model with intrachain interaction J_a , interchain interaction J_{ab} , and DM interaction D_a . By comparing the total energies of the Néel state and the helical state, it is easy to see that in the case of $J_{ab} > \sqrt{J_a^2 + D_a^2} - J_a$, the Néel state has the lower energy. Moreover, we perform MC simulations on a $30 \times 30 \times 1$ supercell with periodic boundary conditions and obtain the phase diagram as shown in Fig. 3. As we expected, the dominant J_{ab} favors the Néel phase. With decreasing J_{ab} , there is a phase transition from the Néel phase to the helical phase, where adjacent helical chains propagate in opposite directions. Interestingly, we find that between the Néel phase and helical phase, there is an intermediate phase in which

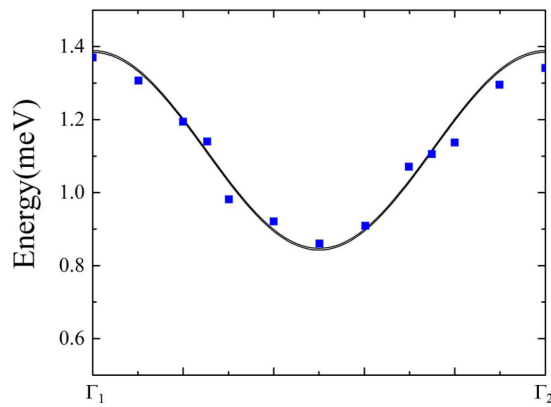


FIG. 4. Calculated spin-wave dispersion along the a^* axis in the fully saturated state ($\mu_0 H = 12$ T) for $\text{K}_2\text{CuSO}_4\text{Cl}_2$. The positions of high-symmetry points in reciprocal lattice units are $\Gamma_1(1, 0, 0)$ and $\Gamma_2(2, 0, 0)$. The inelastic neutron-scattering spectra in Ref. [28] are also shown as discrete points for comparison.

the spins are not lying in the plane perpendicular to D_a , as shown in Fig. 3. In this work, we have $J_{ab}/J_a = 0.01$ and $D_y/J_a = 0.03$ for $\text{K}_2\text{CuSO}_4\text{Cl}_2$, while in the $\text{K}_2\text{CuSO}_4\text{Br}_2$ system, J_{ab}/J_a and D_y/J_a are 0.06 and 0.03, respectively. Thus the magnetic ground states of these two materials are both suggested to be in the Néel phase.

Using linear spin-wave theory, we also calculated the magnetic excitation spectrum of $\text{K}_2\text{CuSO}_4\text{Cl}_2$. The spin-wave dispersion along the high-symmetry axis is shown in Fig. 4.

As a comparison, the inelastic neutron-scattering spectrum in previous experimental work [28] is also shown as blue discrete points. The experimental data from Ref. [28] are at the temperature $T = 1.6$ K with an external magnetic field of $\mu_0 H = 12$ T. Our calculated results are consistent with the experimental measurements.

IV. CONCLUSIONS

In conclusion, we presented a comprehensive investigation of $\text{K}_2\text{CuSO}_4\text{Cl}_2$ and $\text{K}_2\text{CuSO}_4\text{Br}_2$ using first-principles calculations. Our calculations reveal that both compounds are insulators with band gaps of 2.56 and 2.10 eV, respectively. Using the magnetic force theorem and the first-principles linear response method, we calculated the magnetic exchange parameters and the DM interactions, and our calculations are in good agreement with the experiment. We also calculated the magnetic excitation spectrum using linear spin-wave theory, and the results agree well with the experimental inelastic neutron-scattering spectra. Moreover, we used MC simulation to obtain the phase diagram and suggest the ground state of these two materials to be Néel phase.

ACKNOWLEDGMENTS

This work was supported by the National Natural Science Foundation of China (Grants No. 11525417, No. 11834006, No. 51721001, and No. 11790311) and the National Key R&D Program of China (Grants No. 2018YFA0305704 and No. 2017YFA0303203). X.G.W. also acknowledges the support from the Tencent Foundation through the XPLOER PRIZE.

-
- [1] L. Balents, Spin liquids in frustrated magnets, *Nature (London)* **464**, 199 (2010).
- [2] X.-G. Wen, *Quantum Field Theory of Many-Body Systems* (Oxford University Press, New York, 2004).
- [3] R. Coldea, D. Tennant, R. Cowley, D. McMorrow, B. Dorner, and Z. Tylczynski, Neutron scattering study of the magnetic structure of Cs_2CuCl_4 , *J. Phys.: Condens. Matter* **8**, 7473 (1996).
- [4] R. Coldea, D. A. Tennant, R. A. Cowley, D. F. McMorrow, B. Dorner, and Z. Tylczynski, Quasi-1DS = 1/2 Antiferromagnet Cs_2CuCl_4 in a Magnetic Field, *Phys. Rev. Lett.* **79**, 151 (1997).
- [5] R. Coldea, D. A. Tennant, K. Habicht, P. Smeibidl, C. Wolters, and Z. Tylczynski, Direct Measurement of the Spin Hamiltonian and Observation of Condensation of Magnons in the 2D Frustrated Quantum Magnet Cs_2CuCl_4 , *Phys. Rev. Lett.* **88**, 137203 (2002).
- [6] T. Radu, H. Wilhelm, V. Yushankhai, D. Kovrizhin, R. Coldea, Z. Tylczynski, T. Lühmann, and F. Steglich, Bose-Einstein Condensation of Magnons in Cs_2CuCl_4 , *Phys. Rev. Lett.* **95**, 127202 (2005).
- [7] O. A. Starykh, H. Katsura, and L. Balents, Extreme sensitivity of a frustrated quantum magnet: Cs_2CuCl_4 , *Phys. Rev. B* **82**, 014421 (2010).
- [8] Z. Z. Du, H. M. Liu, Y. L. Xie, Q. H. Wang, and J.-M. Liu, Spin Casimir effect in noncollinear quantum antiferromagnets: Torque equilibrium spin wave approach, *Phys. Rev. B* **92**, 214409 (2015).
- [9] T. Ono, H. Tanaka, H. Aruga Katori, F. Ishikawa, H. Mitamura, and T. Goto, Magnetization plateau in the frustrated quantum spin system Cs_2CuBr_4 , *Phys. Rev. B* **67**, 104431 (2003).
- [10] T. Ono, H. Tanaka, O. Kolomyiets, H. Mitamura, T. Goto, K. Nakajima, A. Oosawa, Y. Koike, K. Kakurai, J. Klenke *et al.*, Magnetization plateaux of the $S = 1/2$ two-dimensional frustrated antiferromagnet Cs_2CuBr_4 , *J. Phys.: Condens. Matter* **16**, S773 (2004).
- [11] N. A. Fortune, S. T. Hannahs, Y. Yoshida, T. E. Sherline, T. Ono, H. Tanaka, and Y. Takano, Cascade of Magnetic-Field-Induced Quantum Phase Transitions in a Spin- $1/2$ Triangular-Lattice Antiferromagnet, *Phys. Rev. Lett.* **102**, 257201 (2009).
- [12] S. A. Zvyagin, M. Ozerov, D. Kamenskyi, J. Wosnitza, J. Krzystek, D. Yoshizawa, M. Hagiwara, R. Hu, H. Ryu, C. Petrovic, and M. E. Zhitomirsky, Magnetic excitations in the spin-1/2 triangular-lattice antiferromagnet Cs_2CuBr_4 , *New J. Phys.* **17**, 113059 (2015).
- [13] H.-A. Krug von Nidda, L. E. Svistov, M. V. Eremin, R. M. Eremina, A. Loidl, V. Kataev, A. Validov, A. Prokofiev, and W. Aßmus, Anisotropic exchange in LiCuVO_4 probed by ESR, *Phys. Rev. B* **65**, 134445 (2002).
- [14] B. Gibson, R. Kremer, A. Prokofiev, W. Assmus, and G. McIntyre, Incommensurate antiferromagnetic order in the

- $S = 1/2$ quantum chain compound LiCuVO_4 , *Physica B* **350**, E253 (2004).
- [15] M. Enderle, C. Mukherjee, B. Fåk, R. Kremer, J.-M. Broto, H. Rosner, S.-L. Drechsler, J. Richter, J. Malek, A. Prokofiev *et al.*, Quantum helimagnetism of the frustrated spin-1/2 chain LiCuVO_4 , *Europhys. Lett.* **70**, 237 (2005).
- [16] M. Enderle, B. Fåk, H.-J. Mikeska, R. K. Kremer, A. Prokofiev, and W. Assmus, Two-Spinon and Four-Spinon Continuum in a Frustrated Ferromagnetic Spin-1/2 Chain, *Phys. Rev. Lett.* **104**, 237207 (2010).
- [17] L. Svistov, T. Fujita, H. Yamaguchi, S. Kimura, K. Omura, A. Prokofiev, A. I. Smirnov, Z. Honda, and M. Hagiwara, New high magnetic field phase of the frustrated $S = 1/2$ chain compound LiCuVO_4 , *JETP Lett.* **93**, 21 (2011).
- [18] M. Mourigal, M. Enderle, B. Fåk, R. K. Kremer, J. M. Law, A. Schneidewind, A. Hiess, and A. Prokofiev, Evidence of a Bond-Nematic Phase in LiCuVO_4 , *Phys. Rev. Lett.* **109**, 027203 (2012).
- [19] N. Büttgen, K. Nawa, T. Fujita, M. Hagiwara, P. Kuhns, A. Prokofiev, A. P. Reyes, L. E. Svistov, K. Yoshimura, and M. Takigawa, Search for a spin-nematic phase in the quasi-one-dimensional frustrated magnet LiCuVO_4 , *Phys. Rev. B* **90**, 134401 (2014).
- [20] Z. Z. Du, H. M. Liu, Y. L. Xie, Q. H. Wang, and J.-M. Liu, Magnetic excitations in quasi-one-dimensional helimagnets: Magnon decays and influence of interchain interactions, *Phys. Rev. B* **94**, 134416 (2016).
- [21] A. Orlova, E. L. Green, J. M. Law, D. I. Gorbunov, G. Chanda, S. Krämer, M. Horvatić, R. K. Kremer, J. Wosnitza, and G. L. J. A. Rikken, Nuclear Magnetic Resonance Signature of the Spin-Nematic Phase in LiCuVO_4 at High Magnetic Fields, *Phys. Rev. Lett.* **118**, 247201 (2017).
- [22] S. Nishimoto, S.-L. Drechsler, R. O. Kuzian, J. van den Brink, J. Richter, W. E. A. Lorenz, Y. Skourski, R. Klingeler, and B. Büchner, Saturation Field of Frustrated Chain Cuprates: Broad Regions of Predominant Interchain Coupling, *Phys. Rev. Lett.* **107**, 097201 (2011).
- [23] S. Gangadharaiyah, J. Sun, and O. A. Starykh, Spin-orbital effects in magnetized quantum wires and spin chains, *Phys. Rev. B* **78**, 054436 (2008).
- [24] I. Garate and I. Affleck, Interplay between symmetric exchange anisotropy, uniform Dzyaloshinskii-Moriya interaction, and magnetic fields in the phase diagram of quantum magnets and superconductors, *Phys. Rev. B* **81**, 144419 (2010).
- [25] D. C. Dender, P. R. Hammar, D. H. Reich, C. Broholm, and G. Aeppli, Direct Observation of Field-Induced Incommensurate Fluctuations in a One-Dimensional $S = 1/2$ Antiferromagnet, *Phys. Rev. Lett.* **79**, 1750 (1997).
- [26] T. Masuda, A. Zheludev, K. Uchinokura, J.-H. Chung, and S. Park, Dynamics and Scaling in a Quantum Spin Chain Material with Bond Randomness, *Phys. Rev. Lett.* **93**, 077206 (2004).
- [27] Y.-R. Shu, M. Dupont, D.-X. Yao, S. Capponi, and A. W. Sandvik, Dynamical properties of the $S = \frac{1}{2}$ random Heisenberg chain, *Phys. Rev. B* **97**, 104424 (2018).
- [28] M. Hälgl, W. E. A. Lorenz, K. Y. Povarov, M. Månsson, Y. Skourski, and A. Zheludev, Quantum spin chains with frustration due to Dzyaloshinskii-Moriya interactions, *Phys. Rev. B* **90**, 174413 (2014).
- [29] I. Dzyaloshinsky, A thermodynamic theory of weak ferromagnetism of antiferromagnetics, *J. Phys. Chem. Solids* **4**, 241 (1958).
- [30] T. Moriya, Anisotropic superexchange interaction and weak ferromagnetism, *Phys. Rev.* **120**, 91 (1960).
- [31] W. Jin and O. A. Starykh, Phase diagram of weakly coupled Heisenberg spin chains subject to a uniform Dzyaloshinskii-Moriya interaction, *Phys. Rev. B* **95**, 214404 (2017).
- [32] T. A. Soldatov, A. I. Smirnov, K. Y. Povarov, M. Hälgl, W. E. A. Lorenz, and A. Zheludev, Spin gap in the quasi-one-dimensional $S = \frac{1}{2}$ antiferromagnet $\text{K}_2\text{CuSO}_4\text{Cl}_2$, *Phys. Rev. B* **98**, 144440 (2018).
- [33] D. Blosser, N. Kestin, K. Y. Povarov, R. Bewley, E. Coira, T. Giamarchi, and A. Zheludev, Finite-temperature correlations in a quantum spin chain near saturation, *Phys. Rev. B* **96**, 134406 (2017).
- [34] A. I. Liechtenstein, M. Katsnelson, V. Antropov, and V. Gubanov, Local spin density functional approach to the theory of exchange interactions in ferromagnetic metals and alloys, *J. Magn. Magn. Mater.* **67**, 65 (1987).
- [35] X. Wan, Q. Yin, and S. Y. Savrasov, Calculation of Magnetic Exchange Interactions in Mott-Hubbard Systems, *Phys. Rev. Lett.* **97**, 266403 (2006).
- [36] P. Blaha, K. Schwarz, G. K. Madsen, D. Kvasnicka, and J. Luitz, *WIEN2K, An Augmented Plane Wave+ Local Orbitals Program for Calculating Crystal Properties* (Technische Universität Wien, Wien, 2001).
- [37] V. I. Anisimov, F. Aryasetiawan, and A. Liechtenstein, First-principles calculations of the electronic structure and spectra of strongly correlated systems: The LDA+ U method, *J. Phys.: Condens. Matter* **9**, 767 (1997).
- [38] X. Wan, T. A. Maier, and S. Y. Savrasov, Calculated magnetic exchange interactions in high-temperature superconductors, *Phys. Rev. B* **79**, 155114 (2009).
- [39] A. A. Tsirlin, O. Janson, and H. Rosner, $\beta\text{-Cu}_2\text{V}_2\text{O}_7$: A spin- $\frac{1}{2}$ honeycomb lattice system, *Phys. Rev. B* **82**, 144416 (2010).
- [40] S. Lebernegg, A. A. Tsirlin, O. Janson, and H. Rosner, Spin gap in malachite $\text{Cu}_2(\text{OH})_2\text{CO}_3$ and its evolution under pressure, *Phys. Rev. B* **88**, 224406 (2013).
- [41] O. Janson, I. Rousochatzakis, A. A. Tsirlin, M. Belesi, A. A. Leonov, U. K. Röbber, J. Van Den Brink, and H. Rosner, The quantum nature of skyrmions and half-skyrmions in Cu_2OSeO_3 , *Nat. Commun.* **5**, 5376 (2014).
- [42] D. Koelling and B. Harmon, A technique for relativistic spin-polarised calculations, *J. Phys. C* **10**, 3107 (1977).
- [43] M. Pajda, J. Kudrnovský, I. Turek, V. Drchal, and P. Bruno, *Ab initio* calculations of exchange interactions, spin-wave stiffness constants, and Curie temperatures of Fe, Co, and Ni, *Phys. Rev. B* **64**, 174402 (2001).
- [44] V. V. Mazurenko and V. I. Anisimov, Weak ferromagnetism in antiferromagnets: $\alpha\text{-Fe}_2\text{O}_3$ and La_2CuO_4 , *Phys. Rev. B* **71**, 184434 (2005).
- [45] M. I. Katsnelson, Y. O. Kvashnin, V. V. Mazurenko, and A. I. Liechtenstein, Correlated band theory of spin and orbital contributions to Dzyaloshinskii-Moriya interactions, *Phys. Rev. B* **82**, 100403(R) (2010).

- [46] X. Wan, J. Dong, and S. Y. Savrasov, Mechanism of magnetic exchange interactions in europium monochalcogenides, *Phys. Rev. B* **83**, 205201 (2011).
- [47] D. Wang, X. Bo, F. Tang, and X. Wan, Calculated magnetic exchange interactions in the Dirac magnon material Cu_3TeO_6 , *Phys. Rev. B* **99**, 035160 (2019).
- [48] F. Scordari, E. Scandale, and C. Giacobozzo, The crystal structure of chlorotitionite, $\text{CuK}_2\text{Cl}_2\text{SO}_4$, *Z. Kristallogr.* **144**, 226 (1976).
- [49] W. Jin and O. A. Starykh, DM-induced frustration of the weakly coupled Heisenberg chains, *J. Phys.: Conf. Ser.* **828**, 012019 (2017).